

## Article

# ANADEM: A Digital Terrain Model for South America

Leonardo Laipelt <sup>1,\*</sup>, Bruno Comini de Andrade <sup>1</sup> , Walter Collischonn <sup>1</sup>, Alexandre de Amorim Teixeira <sup>2</sup> ,  
Rodrigo Cauduro Dias de Paiva <sup>1</sup>  and Anderson Ruhoff <sup>1</sup> 

<sup>1</sup> Instituto de Pesquisas Hidráulicas, Universidade Federal do Rio Grande do Sul, Porto Alegre 91501-970, RS, Brazil; anderson.ruhoff@ufrgs.br (A.R.)

<sup>2</sup> Agência Nacional de Águas e Saneamento Básico (ANA), Brasília 70610-200, DF, Brazil; alexandre.amorim@ana.gov.br

\* Correspondence: leonardo.laipelt@ufrgs.br

**Abstract:** Digital elevation models (DEMs) have a wide range of applications and play a crucial role in many studies. Numerous public DEMs, frequently acquired using radar and optical satellite imagery, are currently available; however, DEM datasets tend to exhibit elevation values influenced by vegetation height and coverage, compromising the accuracy of models in representing terrain elevation. In this study, we developed a digital terrain model for South America using a novel methodology to remove vegetation bias in the Copernicus DEM GLO-30 (COPDEM) model using machine learning, Global Ecosystem Dynamics Investigation (GED) elevation data, and multispectral remote sensing products. Our results indicate considerable improvements compared to COPDEM in representing terrain elevation, reducing average errors (BIAS) from 9.6 m to 1.5 m. Furthermore, we evaluated our product (ANADEM) by comparison with other global DEMs, obtaining more accurate results for different conditions of vegetation fraction cover and land use. As a publicly available and open-source dataset, ANADEM will play a crucial role in advancing studies that demand accurate terrain elevation representations at large scales.

**Keywords:** LIDAR; digital elevation model; remote sensing



**Citation:** Laipelt, L.; Comini de Andrade, B.; Collischonn, W.; de Amorim Teixeira, A.; Paiva, R.C.D.d.; Ruhoff, A. ANADEM: A Digital Terrain Model for South America. *Remote Sens.* **2024**, *16*, 2321. <https://doi.org/10.3390/rs16132321>

Academic Editors: Xinghua Li, Qing Cheng and Linwei Yue

Received: 9 April 2024

Revised: 3 June 2024

Accepted: 10 June 2024

Published: 25 June 2024



**Copyright:** © 2024 by the authors. Licensee MDPI, Basel, Switzerland. This article is an open access article distributed under the terms and conditions of the Creative Commons Attribution (CC BY) license (<https://creativecommons.org/licenses/by/4.0/>).

## 1. Introduction

Digital representations of the Earth's surface provide essential data for a wide range of applications, enhancing our understanding of hydrology, landscapes, and terrains, and are key components in many studies, such as topographic mapping [1,2], flood modeling [3–5], landslide analysis [6,7], and atmospheric boundary theory [8].

Digital elevation models (DEMs) can be generated on large scales from different sources, including cartographic data, optical satellite imagery, radar satellite data, and airborne data. At present, satellite data are most commonly used for acquiring digital representations of the Earth's surface, primarily due to their cost-effectiveness and accuracy [9]. Consequently, numerous global or near-global DEMs based on optical and radar satellite data have been made publicly available.

The Shuttle Radar Topography Mission (SRTM) was a pioneering initiative providing the first high-resolution DEM with almost global coverage [10]. SRTM was acquired using a C-radar instrument (31 mm wavelength), which was responsible for populating global topographic information [11]. Subsequently, satellite missions have continued to make significant improvements in terms of the accuracy and spatial resolution of DEMs. Examples include the Advanced Spaceborne Thermal Emission and Reflection Radiometer Global DEM (ASTER GDEM) [12], the Advanced Land Observing Satellite (ALOS) World 3D 30 m (AW3D30) [13], and Copernicus GLO 30 (COPDEM30) [14].

The accuracy of DEMs is significantly influenced by the presence of vegetation [8,15,16], primarily because the most commonly used remote sensing acquisition techniques, such as interferometry (e.g., radar sensors, using X-radar instruments) and stereometry (e.g.,

panchromatic sensors), are unable to capture elevation information for the bare earth surface [17,18]. Consequently, DEMs can be categorized into two types [19]: digital surface models (DSMs), which represent features above the surface, such as vegetation and buildings, and digital terrain models (DTMs), which represent the elevation of the ground surface. Since global DEMs are usually closer to DSMs, numerous studies have sought to develop solutions to mitigate the impact of vegetation bias on global DEMs and to create accurate DTMs [20–24]. Baugh et al. [20] addressed this issue by effectively removing 50–60% of the estimated vegetation height in the SRTM, thereby improving its hydrodynamic modeling accuracy. Applying a similar approach, O’Loughlin et al. [22] incorporated remote sensing products, including vegetation density and height data, into different empirical equations to determine the most effective means of minimizing vegetation bias in the SRTM dataset.

Light detection and ranging data (LiDAR) are not affected by vegetation. Therefore, altitude measured by sensors such as the Global Ecosystem Dynamics Investigation (GEDI) and ICESat (Ice, Cloud, and Land Elevation Satellite) can be considered as the altitude of the terrain. However, because it is not an imaging sensor, information from LiDAR does not have global coverage. For this reason, LiDAR data can only be used to directly correct DEMs in a few pixels. To correct the effect of vegetation on most pixels, the solution that has been adopted is to develop an empirical model that relates the height of the vegetation, or more precisely, the magnitude of the error that the vegetation causes in DEMs [22–24].

For example, Yamazaki et al. [23] introduced The Multi-Error-Removed Improved-Terrain (MERIT) model, which utilized global vegetation databases and LiDAR data from ICESat to reduce vegetation bias in the SRTM model. Similarly, Magruder et al. [24] utilized the differences between SRTM elevations and ICESat-2 terrain heights, canopy cover, and terrain slope to reproduce and remove vegetation biases from the SRTM model.

As the availability of remote sensing data increases and further development of empirical models takes place, the associated increase in complexity may require new approaches. In this context, machine learning advancements have significantly enhanced the utilization of extensive data [25] to create new topographic datasets based on existing remote sensing sources [21,26–29]. Consequently, machine learning has emerged as a powerful tool for generating high-accuracy DTMs comprising large amounts of remote sensing data, including altimetry measurements acquired using LiDAR instruments, such as ICESat and GEDI. For example, Liu et al. [30] used the Random Forest (RF) model to enhance the accuracy of MERIT, resulting in an 18% improvement in flood simulation relative to the original dataset. Additionally, Hawker et al. [21] introduced the Forest and Buildings Removed Copernicus DEM (FABDEM), which mitigates biases from vegetation and urban buildings by applying an RF model and incorporating altimetry data from the GEDI dataset.

Despite some advancements in methodologies to remove vegetation bias in global DEMs, most studies still rely on SRTM, despite the fact that it is outperformed by more recent DEMs [31]. Moreover, the potential of machine learning methods to remove vegetation bias is yet to be fully investigated; many such methods are not yet openly available. This study aims to propose a new DTM for South America, named ANADEM—*Agência Nacional de Águas DEM* (acronym of National Water Agency DEM). First, we developed a methodology to remove vegetation influence using machine learning and remote sensing datasets. To create ANADEM, we selected the COPDEM as the reference DEM due to recent studies identifying it as the most precise freely available global DEM [31–34]. Subsequently, we validated our DTM by comparison with terrain elevation measurements acquired using the ICESat-2 mission and available global DEMs.

ANADEM was developed for applications by the Brazilian water agency and offers several advantages, notably its calibration, which is specifically designed to improve its accuracy over South America. Additionally, we expect that, through using open-source initiatives and freely available data, we will enhance its use in applications requiring topographic information, ensuring easy accessibility to DTM data for South America.

## 2. Methods and Data

### 2.1. Methods Overview

The model workflow in this study was developed to facilitate applicability to different study areas, requiring only terrain elevation and multispectral data to correct vegetation bias from the selected DEM (COPDEM). We applied the model to produce DTM open data for South America (ANADEM) using machine learning and multispectral information from Landsat and Sentinel and elevation profiles from GEDI. The ANADEM algorithm was implemented within the Google Earth Engine (GEE) platform [35] (version 0.1.366) using the JavaScript and Python (version 3.9) APIs. GEE is a cloud platform that provides high-performance computing and easy access to remote sensing data and geoprocessing tools. The scripts utilized to produce ANADEM are available on the GitHub repository (<https://hge-iph.github.io/anadem/> (accessed on 31 May 2024)), along with instructions for running the algorithm.

An overview of the methodology is shown in Figure 1, with further details provided in the subsequent sections.

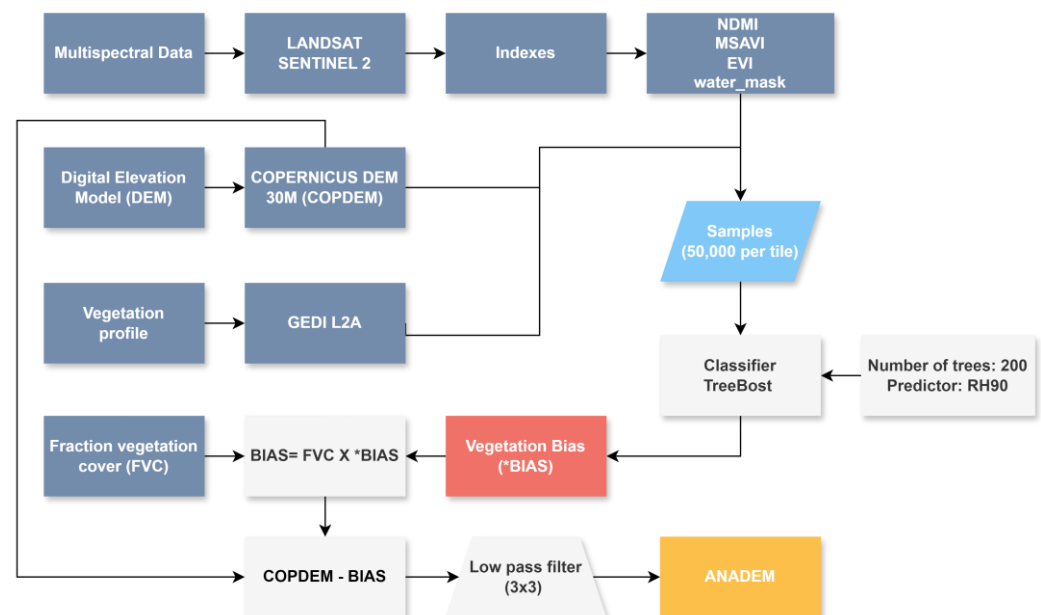


**Figure 1.** Workflow for removing vegetation bias from the COPDEM model. Terrain elevation and multispectral data were used to estimate COPDEM vegetation bias resulting in a new DTM named ANADEM.

### 2.2. Study Area

ANADEM was developed for the continent of South America, which covers an area of 17.8 million km<sup>2</sup> and is characterized by diverse climate and land cover conditions (Figure 2). The region is primarily covered by tropical forests (47%), with extensive areas of pasture, croplands, grasslands, and savannas. The tree structure in South America exhibits substantial variability in canopy density (sparse to dense) and heights, ranging from short (0 to 2 m) to tall (15 to 35 m).

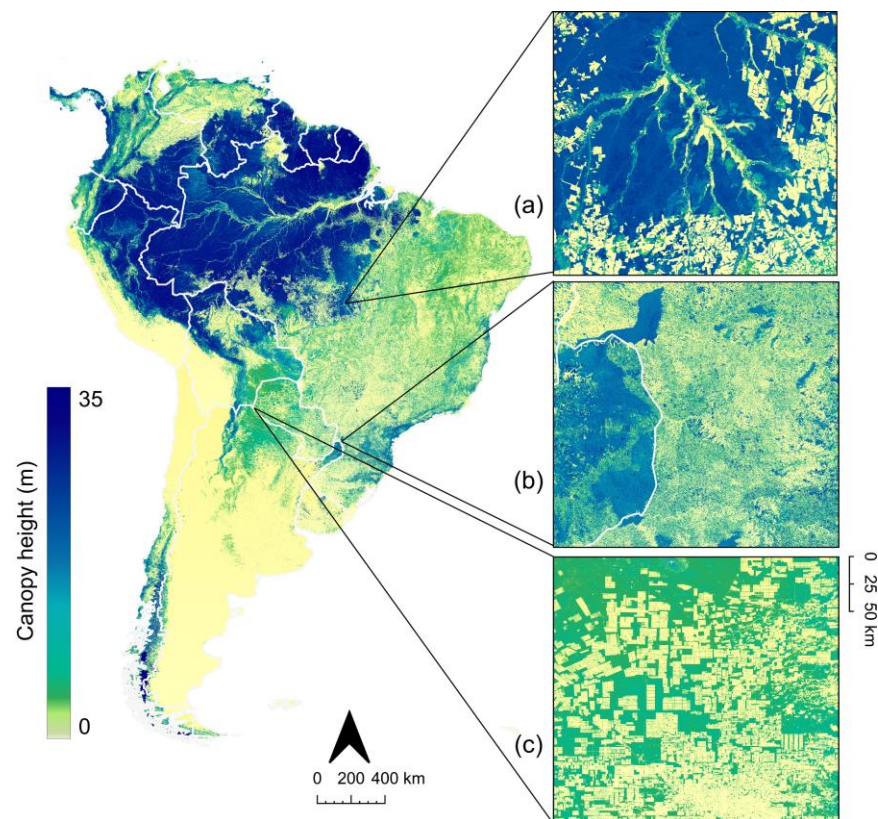


**Figure 2.** Canopy tree height distribution across South America characterized using GEDI and Landsat data [36]. Close-up examples illustrating different canopy heights are shown for the upper Xingu (a), Parana (b), and Paraguay (c) river basins.

### 2.3. COPDEM

The Copernicus GLO-30 (COPDEM) [14] is a resampled version (with a 30 m spatial resolution) derived from the WorldDEM dataset, which is based on radar interferometry data (X-band) acquired by the TanDEM-X mission [37] between 2011 and 2015. Creation of the WorldDEM dataset also involved filling data gaps, incorporating data from other global DEMs, and applying filtering processes. Additional filtering was performed over water bodies by employing a flattening process that ensured a more consistent hydrological network. Recent studies have demonstrated that COPDEM is the most precise freely available global DEM [31–34], motivating its use in this study.

### 2.4. GEDI

The Global Ecosystem Dynamics Investigation (GEDI) is a LiDAR instrument mounted on the International Space Station since 2019. It has a footprint diameter of 25 m and an acquisition data interval of 60 m [38]. GEDI data provide valuable information on canopy structure by measuring the time difference between the emitted and return pulse, this allows the representation of vegetation structure by identifying signals from the ground and the vegetation canopy. The main objective of the GEDI mission is to provide high-accuracy and high global coverage data on canopy structure, which can be used to estimate biomass [39–41] and canopy height [30,38,42].

In this study, GEDI data were acquired from NASA's Earth Data website (<https://search.earthdata.nasa.gov/> (accessed on 27 September 2023)). Elevations and height were derived from the L2A product and referenced to the World Geodetic System 1984 (WGS84) ellipsoid. Then, we obtained the relative height (RH) metrics for each measurement, representing the cumulative energy between the lowest detectable return (ground elevation)



and the highest detectable return (canopy top). To ensure data quality, we applied a filtering process to exclude lower-quality GEDI data points.

### 2.5. Multispectral Data

Multispectral data available between 2013 and 2020 from Landsat and Sentinel were used to compute vegetation indices, which were then integrated into the classifier to capture the vegetation characteristics of the landscape (see Section 3.2). To ensure data quality, a filtering process was implemented to select only images with less than 20% cloud cover.

The Landsat 8 satellite (launched in 2013) was used due to its compatibility with the period of elevation data acquisition from COPDEM. We also selected the highest quality data globally available, from collection 2, which incorporates atmospherically corrected land surface reflectance. The satellite provides high-resolution information (30–100 m) of the Earth’s surface at 16-day intervals, captured by the Operational Land Imager (OLI) and Thermal Infrared Sensor (TIRS) instruments.

Additionally, data from the Sentinel-2 mission, acquired using a pair of satellites equipped with the Multispectral Instrument (MSI), were selected. The spatial resolution of the Sentinel bands ranges from 10 to 60 m. Both satellites operate with a five-day interval between acquisitions.

### 2.6. ICESat-2

ICESat-2 (Ice, Cloud and land Elevation Satellite) was launched in 2018, marking the second generation of satellite missions with the purpose of measuring ice, atmospheric, and topographic parameters via LiDAR measurements [43]. ICESAT-2 is equipped with the Advanced Topographic Laser Altimeter System (ATLAS) which has a footprint diameter of 17 m and a spacing of 90 m between measurements. We obtained data between January 2020 and December 2020, applying the ICESat-2 ATL03 product (<https://icesat-2.gsfc.nasa.gov/> (accessed on 27 September 2023)) to validate our methodology based on independent data. ICESat-2 ATL03 incorporates essential information, such as quality flags and atmospheric and georeferenced corrections, and is also referenced to the WGS84 ellipsoid.

### 2.7. Data Composition

Landsat and Sentinel multispectral data were used to compute spectral indices which were subsequently used as inputs for our model. Spectral indices aggregate spatial information related to vegetation, which generally improves the final results of the classifier. We conducted a preliminary analysis considering different spectral indices and ranked them using the Boruta algorithm [44] which statistically identified the most relevant variables compared to random data. Based on these results, we selected three specific indices, namely the Normalized Difference Moisture Index (NDMI), the Modified Soil Adjusted Vegetation Index (MSAVI), and the Enhanced Vegetation Index (EVI), which demonstrated superior discrimination of vegetation and effectively aggregated information into the model. The detailed equations for each spectral index selected are provided in Table 1. Further details about the variable selection process are provided in Supplementary Material S1.

**Table 1.** Spectral indices and equations used in the model. The indices were computed using the near-infrared (NIR), the short-wave infrared region 1 (SWIR1), the red (R), and the blue (B) bands.

Index	Formula	Satellite	Main Reference
NDMI	$\frac{NIR - SWIR1}{NIR + SWIR1}$	Sentinel	[45]
MSAVI	$2 * NIR + 1 - \sqrt{(2 * NIR + 1)^2 - 8 * (NIR - R)}$	Landsat	[46]
EVI	$\frac{2.5 * (NIR - R)}{(NIR + 6 * R - 7.5 * B) + 1}$	Sentinel	[47]

## 2.8. Vegetation Bias Removal Algorithm

To remove the vegetation bias from the COPDEM product, we used a non-parametric machine learning algorithm, the gradient tree boost classifier [48], which is available on the GEE cloud platform [35]. The gradient tree boost classifier [48] is based on tree decision learning methods and has several advantages over the traditional random forest model due to its optimization techniques (boosting) aimed at minimizing errors in the prediction process. When using this method, each new tree is generated with consideration of the residual errors of the previous tree. Additionally, the gradient tree boost method demonstrated greater robustness than the traditional random forest model in generating accurate results with low sensitivity to outliers and a reduced processing time.

Initially, we divided the study area into 93 ( $5^\circ \times 5^\circ$ ) tiles to avoid processing errors and improve the geographical representativeness of vegetation characteristics. Next, we trained the classifier by randomly selecting 50,000 samples of GEDI points for each tile and extracting the satellite indices values for each point to train the machine learning predictor. The gradient tree boost function available in GEE has different parameters to optimize, including the number of decision trees, shrinkage (which controls the learning rate of the algorithm), the sampling rate for stochastic tree boosting, the maximum number of leaf nodes in each tree, the loss function used for regression, and the number of randomization seeds. We defined the machine learning classifier parameters by testing different optimization settings manually and selecting those with the optimal applicability, highest accuracy, and shortest processing times. As a result, we optimized parameters that exhibited high sensitivity to the results. We applied the gradient tree boost classifier with 200 trees, shrinkage set to 0.1, a sampling rate of 0.6, and selected the Huber statistics as a loss function. For parameters that showed less sensitivity, we used the default values for the maximum number of leaf nodes in each tree (0) and seeds (0).

Results from the classifier were post-processed to correct exaggerated vegetation removal and minimize noise. We utilized the fractional vegetation cover (fvc) mosaic generated with Sentinel-2 multispectral data to ensure that locations with sparse vegetation underwent lower vegetation removal than dense vegetation. Waterbody elevation values remained equal to those used by COPDEM, and an additional step was applied for locations adjacent to water bodies in order to avoid lowered values and ensure hydrological consistency. After subtracting the vegetation bias estimated from the COPDEM, a smoothing focal median filter with a  $3 \times 3$  pixel was applied to reduce noise.

## 2.9. Performance Assessment

To assess the accuracy of the proposed DTM using independent terrain elevation data, we used elevation terrain information obtained by the ICESat-2 satellite. Information from ICESat-2 is available in the 'hf\_best\_fit' band from the ATL03 product, which provides the best-fit ground elevation estimative. We generated a random sample of 20,000 points from ICESat-2 for each tile, these were then compared against other global digital elevation and terrain models, including SRTM, COPDEM, MERIT, and FABDEM.

The following metrics were calculated to enable a statistical assessment of each model evaluated: the root mean squared deviation (RMSE) between the predicted and observed values (Equation (1)), and the mean bias error (BIAS), which is the sum of the differences between the observed and predicted values (Equation (2)).

$$RMSE = \sqrt{\left(\frac{1}{n}\right) \sum_i^n (observed - model)^2} \quad (1)$$

$$BIAS = \frac{1}{n} \sum_i^n (observed - model) \quad (2)$$

### 3. Results and Discussion

#### 3.1. Model Validation

The validation results for vegetation bias removal in the COPDEM model are presented as a new DTM model named ANADEM. Overall, ANADEM led to an 85.6% reduction in vegetation bias compared to COPDEM. Furthermore, disaggregating the results into percentages of tree cover highlights the improvements enabled by removing vegetation bias from COPDEM. For tree cover percentages ranging between 0% and 20%, COPDEM showed an RMSE of 6.40 m and a BIAS of 2.2 m, whereas the RMSE and BIAS of ANADEM were reduced to 5.83 m and 1.67 m, respectively. On the other hand, for areas with greater than 80% tree cover percentage, RMSE and BIAS were reduced from 17.20 and 15.38 m (COPDEM) to 6.94 and 0.25 m (ANADEM). More detailed results in terms of the metrics at different ranges of vegetation cover are presented in Table 2.

**Table 2.** Performance statistics (*BIAS* and *RMSE*) for ANADEM and COPDEM compared to ICESAT-2 data, classified by tree cover intervals. Standard deviation (*STD*) and median values are provided for each tree cover interval.

DEM	Tree Cover (%)	BIAS	RMSE	STD	Median
COPDEM	0 to 20	2.18	6.4	6.02	0.24
	21 to 40	4.06	6.81	5.48	2.42
	41 to 60	8.7	11.61	7.72	6.91
	61 to 80	16.16	18.54	9.09	15.87
	81 to 100	15.38	17.19	7.87	15.77
ANADEM	0 to 20	1.66	5.82	5.58	0.14
	21 to 40	1.76	5.27	4.98	0.84
	41 to 60	2.98	7.98	7.44	2.25
	61 to 80	1.06	8.88	8.83	0.64
	81 to 100	0.25	6.94	7.10	2.25

Previous studies have identified a significant error discrepancy in global DEMs within densely forested areas [49–52], primarily due to sensor limitations when accurately capturing terrain elevation. Li et al. [49] evaluated COPDEM in China, showing an RMSE of 11.9 m with a standard deviation of 8.52 m in regions predominantly covered by dense forests. Similarly, Hawker et al. [52] evaluated three models (MERIT, SRTM, and TanDEM-X) with high-accuracy LiDAR data, showing that all of these models were associated with high RMSE (10–14 m).

Figure 3 shows the error distribution in the ANADEM and COPDEM models in relation to tree cover percentage. For areas with greater than 20% vegetation cover, the benefit of the bias removal performed to generate ANADEM becomes increasingly evident. At approximately 80% vegetation cover, COPDEM results are concentrated around a bias close to 20 m, whereas ANADEM results concentrate at values much closer to zero. This is consistent with the findings of Hawker et al. [21] for COPDEM in areas with canopy cover exceeding 50%, where an RMSE of 26 m was observed. On the other hand, ANADEM was found to be capable of decreasing error differences related to vegetation bias, resulting in a more centered normal distribution.

Furthermore, the findings highlight the importance of accurate DEMs in hydrological modeling, particularly in forested regions where vegetation bias can significantly impact model results [53,54]. The reduced error distribution shown in Figure 3 for ANADEM could lead to more accurate predictions of hydrological processes, which are particularly sensitive to topographic variations [55,56]. It is also noteworthy that, despite the improved performance in areas with dense vegetation, ANADEM showed an increase in negative differences, indicating potential overcorrection in certain instances. This could be attributed to limitations associated with using multispectral data for vegetation bias correction, as variations in vegetation height may not be fully captured in certain conditions. Additionally,

terrain characteristics can influence the model's accuracy, as slope effects may lead to shadowed regions [57], influencing the pixel spectral response.

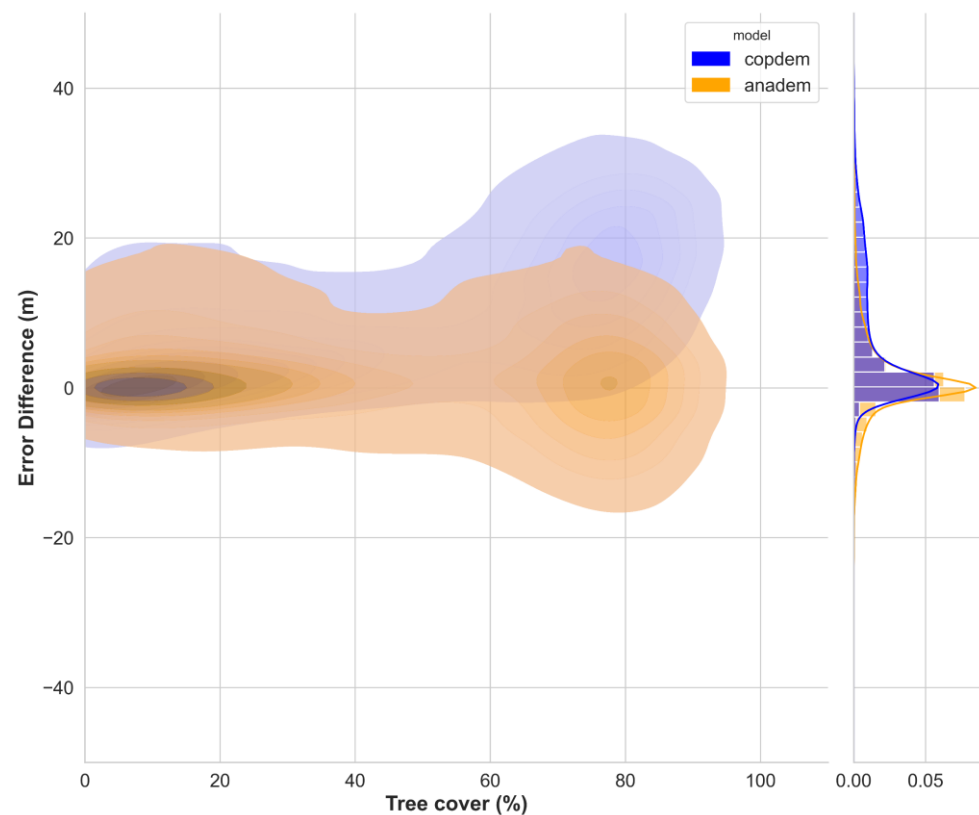


**Figure 3.** Relationship between tree cover percentage and the error difference obtained when comparing COPDEM (blue) and ANADEM (orange) against ICESAT-2 data. Values obtained through the models were based on a sample size of 20,000 for each tile (93 tiles).

### 3.2. Spatial Analysis

To evaluate the spatial results obtained by removing vegetation bias from COPDEM, we selected two areas to illustrate the improvements observed using ANADEM. Figure 4 shows a comparison between the original elevation data from COPDEM, data obtained from ANADEM, and the extracted vegetation bias removed from COPDEM. Overall, ANADEM significantly reduced the influence of vegetation on the elevation values, resulting in a smoother surface than COPDEM. Although certain locations in ANADEM exhibited residual vegetation features due to an underestimation of the vegetation bias, the residual biases were considerably lower than those observed in COPDEM.

Similarly, Figure 5 provides a comparison of results for COPDEM, ANADEM, and the percentage of vegetation removed in an area of the Amazon with extensive land cover changes. The effective removal of vegetation in ANADEM is once again evident, leading to improvements in the representation of the terrain surface, although some vegetation features are still present. Uncertainties in vegetation removal in ANADEM may also occur due to seasonal variations in vegetation, which are influenced by the differences in the time periods of acquisition between COPDEM and multispectral data from satellites used to represent vegetation.



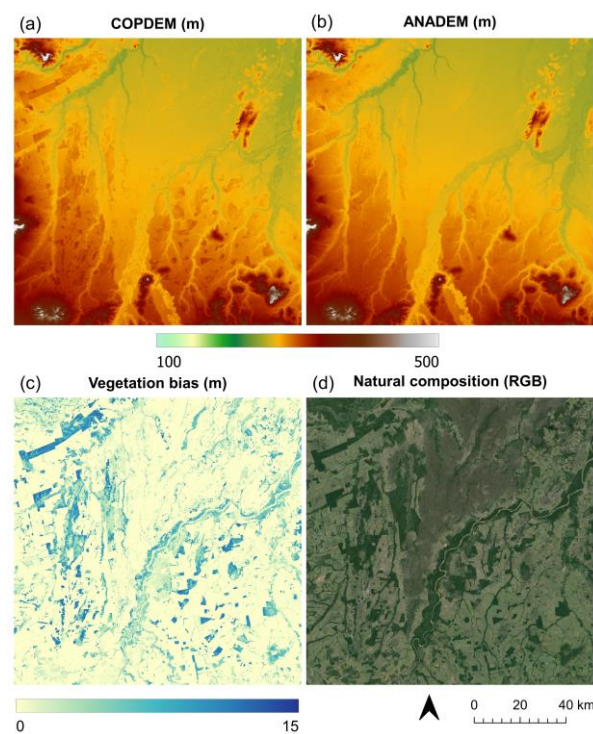


**Figure 4.** Elevation values over the Araguaia basin, Brazil, for COPDEM (a), ANADEM (b), removed vegetation (c), and natural composition (d).

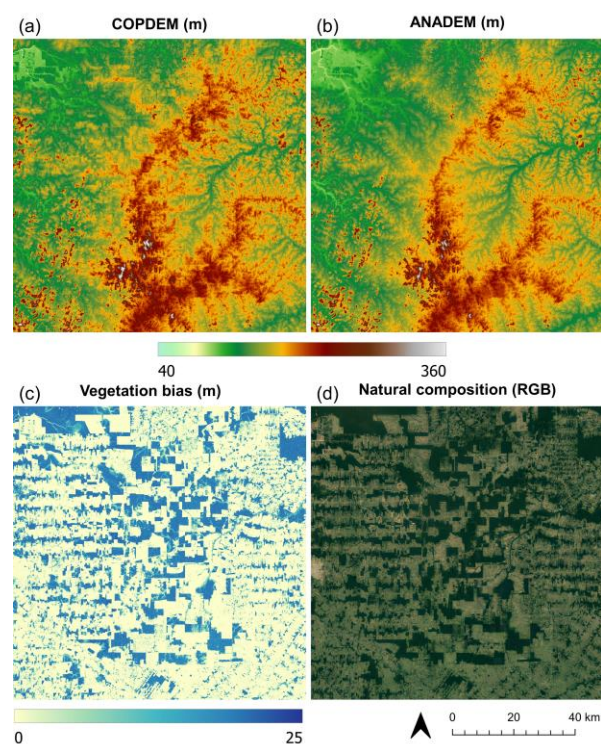


**Figure 5.** Elevation values over mosaic areas of forest, croplands, and pasture areas located in the Amazon, Brazil, for the COPDEM (a), ANADEM (b), the vegetation bias removed (c), and natural composition (d).

### 3.3. Evaluation of Derived Products

DEM inaccuracies can significantly influence the information derived, such as watershed delineation, slope, aspect, and drainage network [56,58]. To evaluate the advances obtained in derived products with ANADEM due to vegetation removal, Figure 6 illustrates an example of watershed delineation (Figure 6a) and drainage network (Figure 6b) obtained from COPDEM and ANADEM compared with a reference basin and drainage network. The watershed delineation and the drainage network for the models were obtained using the TerraHidro software version 5.2.0 provided by the Brazilian National Institute for Space Research (INPE) [59]. Initially, we removed topographic depressions and applied the eight-direction (D8) model to generate a flow direction map and a flow accumulation map. Subsequently, we generated the drainage network by considering a threshold of 5 km<sup>2</sup> of contribution area and finally obtaining the watershed delineation. We utilized the Ottocoded Hydrographic Base (version 5), produced by the Brazilian Water Agency repository (<https://metadados.snirh.gov.br> (accessed on 25 May 2024)), as the reference drainage network and basin (REF).

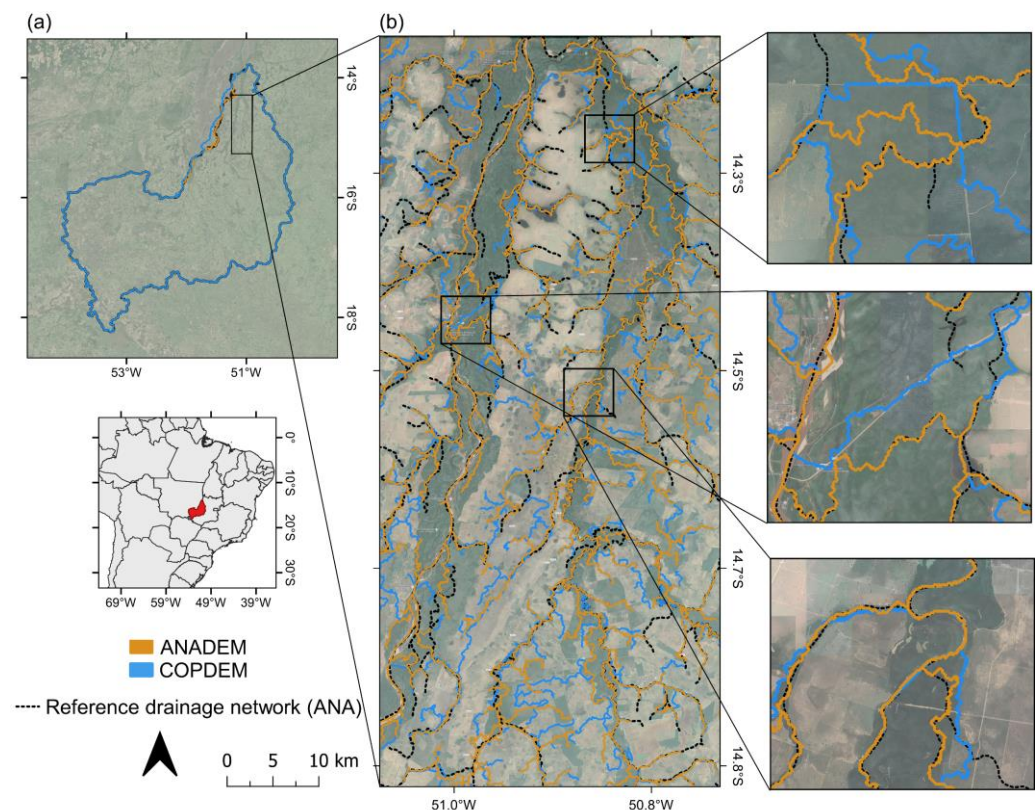


**Figure 6.** Example of the watershed delineation (a) and drainage network (b) extracted from an upper Tocantins-Araguaia sub-basin for COPDEM (blue line) and ANADEM (orange line) compared to the reference drainage network (black dashed line). Results from ANADEM demonstrated enhanced drainage delineation and a reduction in the influence of vegetation and roads.

The quantitative analysis of the derived products indicates that ANADEM produced results closest to the REF, as the estimated basin area was 92,424 km<sup>2</sup>, whereas for ANADEM and COPDEM the delimited area resulted in 92,292 and 93,498 km<sup>2</sup>, respectively. With respect to the basin perimeter, both models showed higher values, with ANADEM and COPDEM obtaining 3336 and 3469 km, respectively, compared to the REF (2647 km). This is expected as the REF basin contour is visually smoother than the ones generated by the models. Additionally, the drainage network density (i.e., total river segment length divided by the basin area) showed that both models have slightly higher drainage densities, obtaining 0.52 km/km<sup>-2</sup> and 0.54 km/km<sup>-2</sup> for ANADEM and COPDEM, respectively,

compared to the REF ( $0.51 \text{ km/km}^{-2}$ ). Other geomorphological characteristics can also be altered due to changes in watershed delineation, such as the length of the main river, the number of segments, aspect, and slope [60,61]. In our example, the differences between the reference length of the main river and the models were 7% and 8%, while the number of segments increased by 10% and 12% for ANADEM and COPDEM, respectively.

Visual inspection also demonstrates that ANADEM-delineated streams are more realistic and smoother than those delineated using COPDEM; this reflected the lower vegetation bias in ANADEM. Common errors in defining drainage networks using DEMs may result from the misinterpretation of flow direction due to objects on the surface acting as ‘barriers’, leading to an inaccurate delineation of the drainage network. Thus, the most significant differences were observed in areas with dense vegetation, which the drainage network computation failed to represent, as shown for COPDEM in Figure 6. This coincides with previous studies demonstrating a loss of drainage delineation accuracy in areas with high vegetation cover [60,62].

The vertical accuracy of both COPDEM and ANADEM is illustrated in Figure 7 in terms of slope (Figure 7a) and aspect (Figure 7b). The vertical error in slope, when compared with ICESat-2 data, showed a proportional increase with increasing slope for both models, although the improvements for ANADEM were more significant. In flat areas (slope  $<3^\circ$ ), ANADEM reduced the error by 84.9% (3.7 m to 0.57 m), whereas on steep slopes ( $>21^\circ$ ), ANADEM reduced the error by 44.5% (from 9.5 m to 5.3 m). For aspect, the errors were practically independent of slope orientation, with the lowest and highest errors observed in the W and NNE directions (5.97 m/6.48 m, respectively), whereas for ANADEM the S and E directions showed the lowest and highest errors (1.30 m/1.63 m, respectively). These results suggest that slope has a greater influence than aspect on the vertical accuracy of DEMs, supporting the conclusions of previous studies [61,63]. Hence, vegetation removal led to a reduction in errors for ANADEM without clearly indicating changes in dependency on slope and aspect.

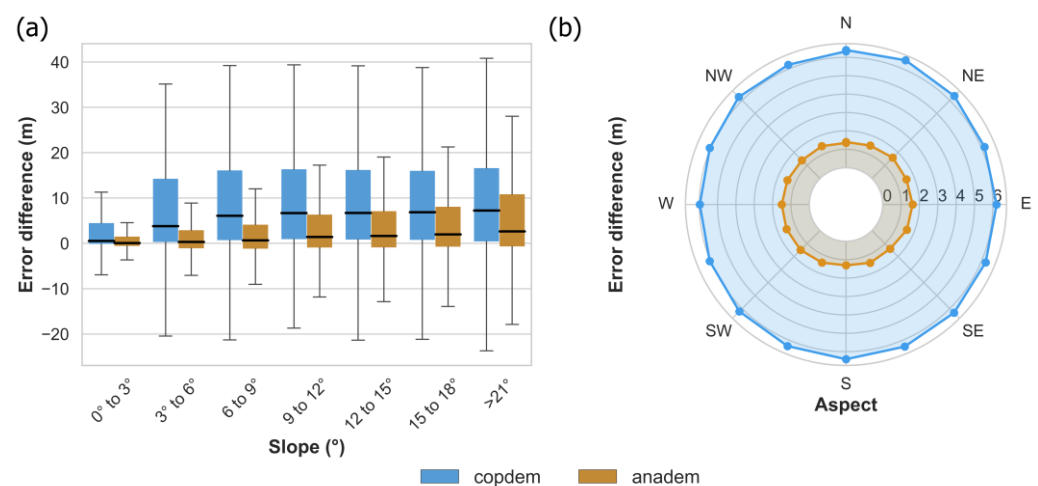


**Figure 7.** Error difference between COPDEM (blue) and ANADEM (orange) compared to ICESAT-2 in terms of slope (a) and aspect (b).

### 3.4. Comparative Assessment with Globally Available Models

The accuracy of ANADEM was compared against terrain elevation from ICESat-2 and four other DEMs available globally. Table 3 shows the performance statistics for each model based on 600,000 randomly selected points. Among the models examined, SRTM and MERIT have the lowest spatial resolutions (90 m), which influences their statistical performance. Canopy structure mainly influences SRTM performance, showing an RMSE of 16.86 m and a bias of 10.33 m. MERIT DEM shows a clear improvement in removing vegetation bias from the SRTM model, reducing RMSE and BIAS to 8.94 m and 3.88 m, respectively. Additionally, COPDEM, with a spatial resolution of 30 m, showed an improve-



ment in accuracy relative to SRTM. Despite the influence of the presence of vegetation, COPDEM results showed an average RMSE of 12.40 m and an average BIAS of 9.56 m.

**Table 3.** Performance statistics (*BIAS* and *RMSE*) for SRTM, COPDEM, MERIT, FABDEM, and ANADEM compared to ICESat-2 data. The standard deviation (*STD*) and median values are provided for each model.

Model	BIAS	RMSE	STD	Median
SRTM	10.33	16.86	12.75	9.28
COPDEM	9.56	12.40	7.24	8.50
MERIT	3.88	8.94	8.00	3.00
FABDEM	1.76	6.81	6.47	0.95
ANADEM	1.50	6.99	6.79	0.75

The FABDEM and ANADEM models presented the lowest errors, denoting a clear improvement in terrain elevation representation compared to other models. The vegetation bias was lowest for ANADEM (1.50 m), whereas FABDEM showed an overestimation of 1.76 m. Our results determined an RMSE of 6.81 m for FABDEM, whereas ANADEM showed a slightly higher RMSE of 6.99 m. The median error compared to ICESat-2 data among the models ranged from 0.75 to 9.28 m. ANADEM exhibited the lowest median error. The average standard deviation error ranged from 6.47 m (FABDEM) to 12.75 m (SRTM).

Figure 8 characterizes the performance metrics into two groups of tree cover percentages. For points classified with less than 50% tree cover (Figure 8a), ANADEM exhibited the lowest error (1.30 m). The errors associated with FABDEM, MERIT, COPDEM, and SRTM were 1.62, 2.16, 2.79, and 4.27 m, respectively. As expected, higher errors were obtained for areas with greater than 50% tree cover. SRTM featured the highest errors (15.78 m), followed by COPDEM (14.85 m). MERIT decreased vegetation bias considerably (5.60 m) despite having a higher value than ANADEM and FABDEM. The most accurate results were obtained by ANADEM and FABDEM, with an average BIAS of 1.49 m and 2.16 m, respectively.

Validation results for each model were also categorized by land cover classes (Table 4) using the MapBiomas classification [64], which is available at a spatial resolution of 30 m for Brazil. Results were obtained for the most representative classes of the study area, totaling six classes: forests, urban areas, savannas, croplands, grasslands, and pastures. The highest bias was observed for forested areas, ranging from 0.4 m (ANADEM) to 14.31 m (COPDEM). ANADEM showed the lowest bias in pastures (1.42 m), grasslands (0.45 m), croplands (0.36 m), and forests, whereas FABDEM showed better results for savannas (2.17 m) and urban areas (0.17 m). The percentage RMSE for ANADEM varied from 2.26 m (croplands) to 7.09 m (forests), whereas those for COPDEM varied between 2.39 (croplands) and 16.44 m (forests). In urban areas, despite the lack of application of a specific bias correction caused by buildings in ANADEM, its performance metrics were slightly better than those of COPDEM. This may be attributed to the post-processing adopted in ANADEM to reduce noise generated by the machine learning model. Additionally, MERIT exhibited a lower performance relative to COPDEM in certain classifications, for example, croplands, grasslands, pastures, and urban areas.

**Table 4.** Validation results for SRTM, COPDEM, MERIT, FABDEM, and ANADEM for the main land cover classes identified in the study area (MapBiomas classification).

Land Cover	Model	BIAS	RMSE	%RMSE	STD	Median
Pastures (n = 54,242)	SRTM	5.37	10.85	2.95	9.42	3.34
	COPDEM	2.1	5.33	1.45	4.89	0.45
	MERIT	2.67	6.27	1.7	5.67	1.77
	FABDEM	1.88	4.95	1.34	4.57	0.45
	ANADEM	1.42	4.7	1.28	4.48	0.23

Table 4. Cont.

Land Cover	Model	BIAS	RMSE	%RMSE	STD	Median
Grasslands (n = 12,073)	SRTM	2.61	6.71	2.87	6.18	2.19
	COPDEM	1.26	3.81	1.63	3.59	0.27
	MERIT	1.66	4.54	1.94	4.22	1.44
	FABDEM	0.97	3.41	1.46	3.27	0.27
	ANADEM	0.45	3.39	1.45	3.36	−0.01
Croplands (n = 18,389)	SRTM	2.81	5.93	1.18	5.22	2.15
	COPDEM	0.54	2.39	0.47	2.33	0.07
	MERIT	1.72	3.57	0.71	3.12	1.5
	FABDEM	0.5	2.33	0.46	2.28	0.06
	ANADEM	0.36	2.26	0.45	2.23	0.0
Savanna (n = 33,461)	SRTM	4.53	8.99	2.25	7.76	3.79
	COPDEM	3.08	5.18	1.29	4.16	1.98
	MERIT	2.95	5.99	1.5	5.21	2.33
	FABDEM	2.17	4.49	1.12	3.93	1.23
	ANADEM	2.35	4.75	1.18	4.12	1.46
Forests (n = 100,690)	SRTM	13.78	17.32	8.35	10.48	13.77
	COPDEM	14.31	16.44	7.93	8.09	14.32
	MERIT	4.69	8.89	4.28	7.55	4.36
	FABDEM	0.83	6.83	3.29	6.78	0.97
	ANADEM	0.4	7.09	3.42	7.08	0.25
Urban areas (n = 1228)	SRTM	3.7	6.94	1.65	5.87	3.05
	COPDEM	2.01	4.01	0.95	3.47	1.25
	MERIT	2.78	5.08	1.2	4.25	2.26
	FABDEM	0.17	3.53	0.84	3.53	−0.16
	ANADEM	1.83	3.78	0.9	3.31	1.18

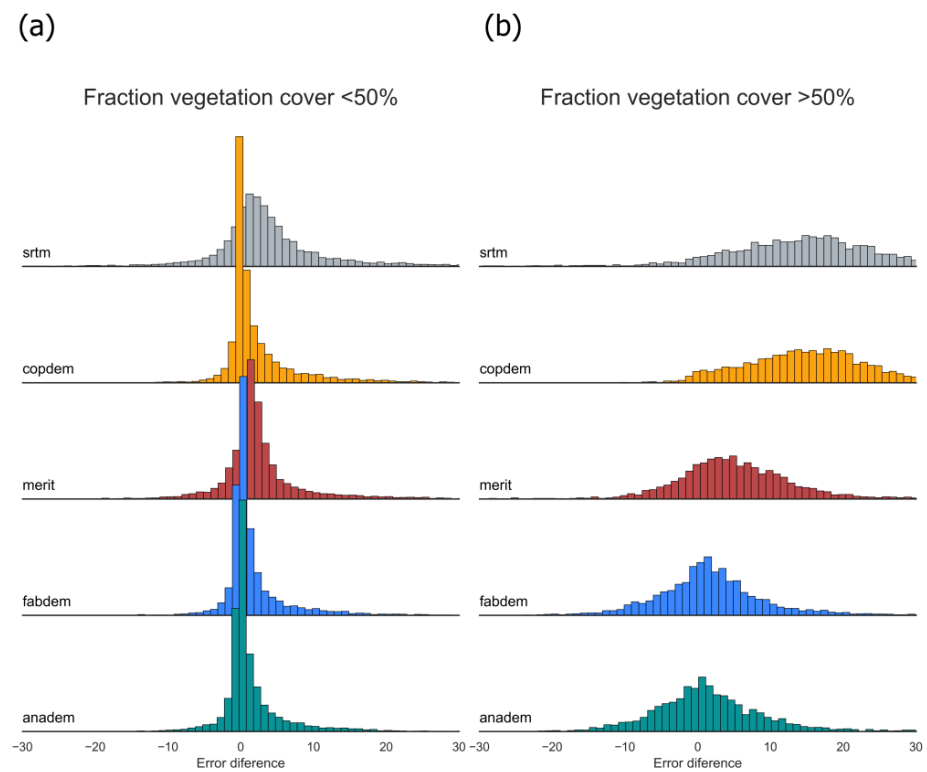


**Figure 8.** Histograms comparing SRTM, COPDEM, MERIT, FABDEM, and ANADEM against ICESat2 altimetry measurements for 600,000 points randomly sampled across South America. Results for ICESat-2 points classified with less than 50% (a) and greater than 50% tree cover (b).



#### 4. Conclusions

In this study, we presented ANADEM, a DTM for South America based on a solution to remove the influence of vegetation on elevation values from COPDEM. ANADEM integrates remote sensing data, cloud computation, and machine learning techniques. According to our findings, ANADEM reduced 85.6% of the vegetation effect relative to COPDEM, while also exhibiting accurate results in comparison with other models. Because vegetation influences derived products, additional benefits over COPDEM were observed when obtaining watershed delineation and drainage networks from ANADEM.

Several concluding points should be emphasized. Firstly, the accuracy of ANADEM results is directly impacted by the terrain elevation values used for model training as well as by the multispectral data representing vegetation. Although we utilized publicly available high-quality data in our study, errors may arise in areas with high cloud cover or inconsistent terrain elevation values from ICESat-2; these may introduce uncertainties in vegetation removal. Secondly, the parameters and temporal data period used to generate ANADEM were defined to facilitate vegetation removal on a continental scale, which could result in inconsistencies due to temporal differences in data acquisition. In such cases, users are encouraged to reproduce the proposed methodology by incorporating adaptations for smaller scales and by selecting multispectral data that align with the vegetation bias observed in COPDEM. Finally, we did not apply bias corrections for urban areas due to a perceived lack of publicly available datasets for model training that accurately represent buildings.

Future studies should aim to better understand the biases introduced by the presence of buildings and explore methods of bias identification without losing terrain characteristics. Moreover, with the increasing availability of high-resolution LiDAR DEMs for South America, there is an opportunity for further enhancement through the potential integration of these data into the algorithm, as well as its utilization for validation purposes.

ANADEM data are freely available to users, and we anticipate that the proposed methods may enable new advancements in hydrological and surface modeling in South America. Additionally, ANADEM may facilitate the development of new products based on the scripts utilized in this study for removing vegetation bias from DEM models.

**Supplementary Materials:** The following supporting information can be downloaded at: <https://www.mdpi.com/article/10.3390/rs16132321/s1>, Table S1: Candidate variables analyzed for vegetation bias removal in South America; Table S2: Index formulas and inputs.; Table S3: Selected variables resulting from the Boruta algorithm correlation analysis application [44,65].

**Author Contributions:** Conceptualization, L.L., B.C.d.A. and A.R.; methodology, L.L., B.C.d.A. and A.R.; software, L.L. and B.C.d.A.; investigation, L.L., A.R., B.C.d.A., W.C., R.C.D.d.P. and A.d.A.T.; writing—original draft preparation, L.L.; writing—review and editing, A.R., B.C.d.A., W.C., R.C.D.d.P. and A.d.A.T.; supervision, A.R., W.C., R.C.D.d.P. and A.d.A.T.; project administration, A.R.; funding acquisition, R.C.D.d.P. and A.d.A.T. All authors have read and agreed to the published version of the manuscript.

**Funding:** This research was financially supported by the Brazilian Water Agency (ANA) in the context of the research project “Cooperation in technologies for hydrological analysis on a national scale”, grant number TED-05/2019-ANA.

**Data Availability Statement:** The data generated in this study are freely available for use on different platforms. Users can access the latest version of ANADEM in the Google Earth Engine (projects/et-brasil/assets/anadem/v1), and can download the data separated into Military Grid Reference System (MGRS) tiles on the GitHub repository (<https://hge-iph.github.io/anadem/> (accessed on 31 May 2024)). We also encourage users to access the source code used to develop ANADEM, which is also available on the GitHub repository.

**Acknowledgments:** The authors gratefully acknowledge the Brazilian National Council for Scientific and Technological Development (CNPq). The authors are also grateful for the support of the Google Earth Engine team and additionally acknowledge the European Space Agency (ESA) for providing free access to the Copernicus GLO-30 DEM.

**Conflicts of Interest:** The authors declare no conflicts of interest.

## References

- Schumann, G.; Matgen, P.; Cutler, M.E.J.; Black, A.; Hoffmann, L.; Pfister, L. Comparison of Remotely Sensed Water Stages from LiDAR, Topographic Contours and SRTM. *ISPRS J. Photogramm. Remote Sens.* **2008**, *63*, 283–296. [\[CrossRef\]](#)
- Fluet-Chouinard, E.; Lehner, B.; Rebelo, L.M.; Papa, F.; Hamilton, S.K. Development of a Global Inundation Map at High Spatial Resolution from Topographic Downscaling of Coarse-Scale Remote Sensing Data. *Remote Sens. Environ.* **2015**, *158*, 348–361. [\[CrossRef\]](#)
- Fleischmann, A.S.; Papa, F.; Hamilton, S.K.; Fassoni-Andrade, A.; Wongchuig, S.; Espinoza, J.-C.; Paiva, R.C.D.; Melack, J.M.; Fluet-Chouinard, E.; Castello, L.; et al. Increased Floodplain Inundation in the Amazon since 1980. *Environ. Res. Lett.* **2023**, *18*, 34024. [\[CrossRef\]](#)
- Rangari, V.A.; Umamahesh, N.V.; Bhatt, C.M. Assessment of Inundation Risk in Urban Floods Using HEC RAS 2D. *Model. Earth Syst. Environ.* **2019**, *5*, 1839–1851. [\[CrossRef\]](#)
- Kulp, S.; Strauss, B.H. Global DEM Errors Underpredict Coastal Vulnerability to Sea Level Rise and Flooding. *Front. Earth Sci.* **2016**, *4*, 36. [\[CrossRef\]](#)
- Pike, R.J. The Geometric Signature: Quantifying Landslide-Terrain Types from Digital Elevation Models. *Math. Geol.* **1988**, *20*, 491–511. [\[CrossRef\]](#)
- Ji, S.; Yu, D.; Shen, C.; Li, W.; Xu, Q. Landslide Detection from an Open Satellite Imagery and Digital Elevation Model Dataset Using Attention Boosted Convolutional Neural Networks. *Landslides* **2020**, *17*, 1337–1352. [\[CrossRef\]](#)
- Okolie, C.J.; Smit, J.L. A Systematic Review and Meta-Analysis of Digital Elevation Model (DEM) Fusion: Pre-Processing, Methods and Applications. *ISPRS J. Photogramm. Remote Sens.* **2022**, *188*, 1–29. [\[CrossRef\]](#)
- Kayadibi, O. Recent Advances in Satellite Technologies Using to Generate the Digital Elevation Model (DEM). In Proceedings of the 2009 4th International Conference on Recent Advances in Space Technologies, Istanbul, Turkey, 11–13 June 2009; pp. 380–385.
- Farr, T.G.; Rosen, P.A.; Caro, E.; Crippen, R.; Duren, R.; Hensley, S.; Kobrick, M.; Paller, M.; Rodriguez, E.; Roth, L.; et al. The Shuttle Radar Topography Mission. *Rev. Geophys.* **2007**, *45*, RG2004. [\[CrossRef\]](#)
- van Zyl, J.J. The Shuttle Radar Topography Mission (SRTM): A Breakthrough in Remote Sensing of Topography. *Acta Astronaut.* **2001**, *48*, 559–565. [\[CrossRef\]](#)
- Abrams, M.; Hook, S.; Ramachandran, B. ASTER User Handbook, Version 2. *Jet Propuls. Lab.* **2002**, *4800*, 135.
- Tadono, T.; Ishida, H.; Oda, F.; Naito, S.; Minakawa, K.; Iwamoto, H. Precise Global DEM Generation by ALOS PRISM. *ISPRS Ann. Photogramm. Remote Sens. Spat. Inf. Sci.* **2014**, *2*, 71–76. [\[CrossRef\]](#)
- AIRBUS Copernicus DEM: Copernicus Digital Elevation Model Product Handbook; Report AO/1-9422/18/IL G; Airbus Defence and Space GmbH: Taufkirchen, Germany, 2020.
- Thomas, J.; Joseph, S.; Thirvikramji, K.P.; Arunkumar, K.S. Sensitivity of Digital Elevation Models: The Scenario from Two Tropical Mountain River Basins of the Western Ghats, India. *Geosci. Front.* **2014**, *5*, 893–909. [\[CrossRef\]](#)
- Kenward, T.; Lettenmaier, D.P.; Wood, E.F.; Fielding, E. Effects of Digital Elevation Model Accuracy on Hydrologic Predictions. *Remote Sens. Environ.* **2000**, *74*, 432–444. [\[CrossRef\]](#)
- Zhu, J.; Xie, Y.; Fu, H.; Wang, C.; Wang, H.; Liu, Z.; Xie, Q. Digital Terrain, Surface, and Canopy Height Model Generation with Dual-Baseline Low-Frequency InSAR over Forest Areas. *J. Geod.* **2023**, *97*, 100. [\[CrossRef\]](#)
- Schlund, M.; Baron, D.; Magdon, P.; Erasmi, S. Canopy Penetration Depth Estimation with TanDEM-X and Its Compensation in Temperate Forests. *ISPRS J. Photogramm. Remote Sens.* **2019**, *147*, 232–241. [\[CrossRef\]](#)
- Guth, P.L.; Van Niekerk, A.; Grohmann, C.H.; Muller, J.-P.; Hawker, L.; Florinsky, I.V.; Gesch, D.; Reuter, H.I.; Herrera-Cruz, V.; Riazanoff, S.; et al. Digital Elevation Models: Terminology and Definitions. *Remote Sens.* **2021**, *13*, 3581. [\[CrossRef\]](#)
- Baugh, C.A.; Bates, P.D.; Schumann, G.; Trigg, M.A. SRTM Vegetation Removal and Hydrodynamic Modeling Accuracy. *Water Resour. Res.* **2013**, *49*, 5276–5289. [\[CrossRef\]](#)
- Hawker, L.; Uhe, P.; Paulo, L.; Sosa, J.; Savage, J.; Sampson, C.; Neal, J. A 30 m Global Map of Elevation with Forests and Buildings Removed. *Environ. Res. Lett.* **2022**, *17*, 24016. [\[CrossRef\]](#)
- O'Loughlin, F.E.; Paiva, R.C.D.; Durand, M.; Alsdorf, D.E.; Bates, P.D. A Multi-Sensor Approach towards a Global Vegetation Corrected SRTM DEM Product. *Remote Sens. Environ.* **2016**, *182*, 49–59. [\[CrossRef\]](#)
- Yamazaki, D.; Ikeshima, D.; Tawatari, R.; Yamaguchi, T.; O'Loughlin, F.; Neal, J.C.; Sampson, C.C.; Kanae, S.; Bates, P.D. A High-Accuracy Map of Global Terrain Elevations. *Geophys. Res. Lett.* **2017**, *44*, 5844–5853. [\[CrossRef\]](#)
- Magruder, L.; Neuenschwander, A.; Klotz, B. Digital Terrain Model Elevation Corrections Using Space-Based Imagery and ICESat-2 Laser Altimetry. *Remote Sens. Environ.* **2021**, *264*, 112621. [\[CrossRef\]](#)
- Li, L.; Han, L.; Ding, M.; Cao, H.; Hu, H. A Deep Learning Semantic Template Matching Framework for Remote Sensing Image Registration. *ISPRS J. Photogramm. Remote Sens.* **2021**, *181*, 205–217. [\[CrossRef\]](#)
- Liu, Y.; Bates, P.D.; Neal, J.C.; Yamazaki, D. Bare-Earth DEM Generation in Urban Areas for Flood Inundation Simulation Using Global Digital Elevation Models. *Water Resour. Res.* **2021**, *57*, e2020WR028516. [\[CrossRef\]](#)
- Manfreda, S.; Samela, C. A Digital Elevation Model Based Method for a Rapid Estimation of Flood Inundation Depth. *J. Flood Risk Manag.* **2019**, *12*, e12541. [\[CrossRef\]](#)

28. Mao, X.; Chow, J.K.; Su, Z.; Wang, Y.-H.; Li, J.; Wu, T.; Li, T. Deep Learning-Enhanced Extraction of Drainage Networks from Digital Elevation Models. *Environ. Model. Softw.* **2021**, *144*, 105135. [\[CrossRef\]](#)
29. Wendi, D.; Liong, S.-Y.; Sun, Y.; Doan, C.D. An Innovative Approach to Improve SRTM DEM Using Multispectral Imagery and Artificial Neural Network. *J. Adv. Model. Earth Syst.* **2016**, *8*, 691–702. [\[CrossRef\]](#)
30. Liu, X.; Su, Y.; Hu, T.; Yang, Q.; Liu, B.; Deng, Y.; Tang, H.; Tang, Z.; Fang, J.; Guo, Q. Neural Network Guided Interpolation for Mapping Canopy Height of China's Forests by Integrating GEDI and ICESat-2 Data. *Remote Sens. Environ.* **2022**, *269*, 112844. [\[CrossRef\]](#)
31. Bielski, C.; López-Vázquez, C.; Grohmann, C.H.; Guth, P.L.; Hawker, L.; Gesch, D.; Trevisani, S.; Herrera-Cruz, V.; Riazanoff, S.; Corseaux, A.; et al. Novel Approach for Ranking DEMs: Copernicus DEM Improves One Arc Second Open Global Topography. *IEEE Trans. Geosci. Remote Sens.* **2024**, *62*, 4503922. [\[CrossRef\]](#)
32. Li, J.; Zhao, Y.; Bates, P.; Neal, J.; Tooth, S.; Hawker, L.; Maffei, C. Digital Elevation Models for Topographic Characterisation and Flood Flow Modelling along Low-Gradient, Terminal Dryland Rivers: A Comparison of Spaceborne Datasets for the Río Colorado, Bolivia. *J. Hydrol.* **2020**, *591*, 125617. [\[CrossRef\]](#)
33. Guth, P.L.; Geoffroy, T.M. LiDAR Point Cloud and ICESat-2 Evaluation of 1 Second Global Digital Elevation Models: Copernicus Wins. *Trans. GIS* **2021**, *25*, 2245–2261. [\[CrossRef\]](#)
34. Purinton, B.; Bookhagen, B. Beyond Vertical Point Accuracy: Assessing Inter-Pixel Consistency in 30 m Global DEMs for the Arid Central Andes. *Front. Earth Sci.* **2021**, *9*, 758606. [\[CrossRef\]](#)
35. Gorelick, N.; Hancher, M.; Dixon, M.; Ilyushchenko, S.; Thau, D.; Moore, R. Google Earth Engine: Planetary-Scale Geospatial Analysis for Everyone. *Remote Sens. Environ.* **2017**, *202*, 18–27. [\[CrossRef\]](#)
36. Potapov, P.; Li, X.; Hernandez-Serna, A.; Tyukavina, A.; Hansen, M.C.; Kommareddy, A.; Pickens, A.; Turubanova, S.; Tang, H.; Silva, C.E.; et al. Mapping Global Forest Canopy Height through Integration of GEDI and Landsat Data. *Remote Sens. Environ.* **2021**, *253*, 112165. [\[CrossRef\]](#)
37. Zink, M.; Fiedler, H.; Hajnsek, I.; Krieger, G.; Moreira, A.; Werner, M. The TanDEM-X Mission Concept. In Proceedings of the 2006 IEEE International Symposium on Geoscience and Remote Sensing, Denver, CO, USA, 31 July–4 August 2006; pp. 1938–1941.
38. Dubayah, R.; Blair, J.B.; Goetz, S.; Fatoyinbo, L.; Hansen, M.; Healey, S.; Hofton, M.; Hurtt, G.; Kellner, J.; Luthcke, S.; et al. The Global Ecosystem Dynamics Investigation: High-Resolution Laser Ranging of the Earth's Forests and Topography. *Sci. Remote Sens.* **2020**, *1*, 100002. [\[CrossRef\]](#)
39. Qin, Y.; Xiao, X.; Wigneron, J.-P.; Ciais, P.; Brandt, M.; Fan, L.; Li, X.; Crowell, S.; Wu, X.; Doughty, R.; et al. Carbon Loss from Forest Degradation Exceeds That from Deforestation in the Brazilian Amazon. *Nat. Clim. Change* **2021**, *11*, 442–448. [\[CrossRef\]](#)
40. Duncanson, L.; Kellner, J.R.; Armston, J.; Dubayah, R.; Minor, D.M.; Hancock, S.; Healey, S.P.; Patterson, P.L.; Saarela, S.; Marselis, S.; et al. Aboveground Biomass Density Models for NASA's Global Ecosystem Dynamics Investigation (GEDI) Lidar Mission. *Remote Sens. Environ.* **2022**, *270*, 112845. [\[CrossRef\]](#)
41. Santoro, M.; Cartus, O.; Carvalhais, N.; Rozendaal, D.M.A.; Avitabile, V.; Araza, A.; de Bruin, S.; Herold, M.; Quegan, S.; Rodríguez-Veiga, P.; et al. The Global Forest Above-Ground Biomass Pool for 2010 Estimated from high-Resolution Satellite Observations. *Earth Syst. Sci. Data* **2021**, *13*, 3927–3950. [\[CrossRef\]](#)
42. Lang, N.; Kalischek, N.; Armston, J.; Schindler, K.; Dubayah, R.; Wegner, J.D. Global Canopy Height Regression and Uncertainty Estimation from GEDI LIDAR Waveforms with Deep Ensembles. *Remote Sens. Environ.* **2022**, *268*, 112760. [\[CrossRef\]](#)
43. Palm, S.; Yang, Y.; Herzfeld, U.; Hancock, D. *ICESat-2 Algorithm Theoretical Basis Document for the Atmosphere, Part I: Level 2 and 3 Data Products*; National Aeronautics and Space Administration, Goddard Space Flight Center: Glenn Dale, MD, USA, 2018.
44. Kursu, M.B.; Rudnicki, W.R. Feature Selection with the Boruta Package. *J. Stat. Softw.* **2010**, *36*, 1–13. [\[CrossRef\]](#)
45. Gao, B. NDWI—A Normalized Difference Water Index for Remote Sensing of Vegetation Liquid Water from Space. *Remote Sens. Environ.* **1996**, *58*, 257–266. [\[CrossRef\]](#)
46. Qi, J.; Chehbouni, A.; Huete, A.R.; Kerr, Y.H.; Sorooshian, S. A Modified Soil Adjusted Vegetation Index. *Remote Sens. Environ.* **1994**, *48*, 119–126. [\[CrossRef\]](#)
47. Liu, H.Q.; Huete, A. A Feedback Based Modification of the NDVI to Minimize Canopy Background and Atmospheric Noise. *IEEE Trans. Geosci. Remote Sens.* **1995**, *33*, 457–465. [\[CrossRef\]](#)
48. Friedman, J.H. Greedy Function Approximation: A Gradient Boosting Machine. *Ann. Stat.* **2001**, *29*, 1189–1232.
49. Li, H.; Zhao, J.; Yan, B.; Yue, L.; Wang, L. Global DEMs Vary from One to Another: An Evaluation of Newly Released Copernicus, NASA and AW3D30 DEM on Selected Terrains of China Using ICESat-2 Altimetry Data. *Int. J. Digit. Earth* **2022**, *15*, 1149–1168. [\[CrossRef\]](#)
50. Ludwig, R.; Schneider, P. Validation of Digital Elevation Models from SRTM X-SAR for Applications in Hydrologic Modeling. *ISPRS. J. Photogramm. Remote Sens.* **2006**, *60*, 339–358. [\[CrossRef\]](#)
51. Gdulová, K.; Marešová, J.; Moudrý, V. Accuracy Assessment of the Global TanDEM-X Digital Elevation Model in a Mountain Environment. *Remote Sens. Environ.* **2020**, *241*, 111724. [\[CrossRef\]](#)
52. Hawker, L.; Neal, J.; Bates, P. Accuracy Assessment of the TanDEM-X 90 Digital Elevation Model for Selected Floodplain Sites. *Remote Sens. Environ.* **2019**, *232*, 111319. [\[CrossRef\]](#)
53. Carabajal, C.C.; Harding, D.J. ICESat Validation of SRTM C-Band Digital Elevation Models. *Geophys. Res. Lett.* **2005**, *32*, L22S01. [\[CrossRef\]](#)

54. Jarihani, A.A.; Callow, J.N.; McVicar, T.R.; Van Niel, T.G.; Larsen, J.R. Satellite-Derived Digital Elevation Model (DEM) Selection, Preparation and Correction for Hydrodynamic Modelling in Large, Low-Gradient and Data-Sparse Catchments. *J. Hydrol.* **2015**, *524*, 489–506. [CrossRef]
55. Lin, K.; Zhang, Q.; Chen, X. An Evaluation of Impacts of DEM Resolution and Parameter Correlation on TOPMODEL Modeling Uncertainty. *J. Hydrol.* **2010**, *394*, 370–383. [CrossRef]
56. Wechsler, S.P. Uncertainties Associated with Digital Elevation Models for Hydrologic Applications: A Review. *Hydrol. Earth Syst. Sci.* **2007**, *11*, 1481–1500. [CrossRef]
57. Isikdogan, F.; Bovik, A.C.; Passalacqua, P. Surface Water Mapping by Deep Learning. *IEEE J. Sel. Top. Appl. Earth Obs. Remote Sens.* **2017**, *10*, 4909–4918. [CrossRef]
58. Goulden, T.; Hopkinson, C.; Jamieson, R.; Sterling, S. Sensitivity of DEM, Slope, Aspect and Watershed Attributes to LiDAR Measurement Uncertainty. *Remote Sens. Environ.* **2016**, *179*, 23–35. [CrossRef]
59. TerraHidro. Available online: <https://www.dpi.inpe.br/terrahidro/doku.php?id=start&rev=1704159885> (accessed on 20 September 2023).
60. Thommeret, N.; Bailly, J.S.; Puech, C. Extraction of Thalweg Networks from DTMs: Application to Badlands. *Hydrol. Earth Syst. Sci.* **2010**, *14*, 1527–1536. [CrossRef]
61. Uuemaa, E.; Ahi, S.; Montibeller, B.; Muru, M.; Knoch, A. Vertical Accuracy of Freely Available Global Digital Elevation Models (ASTER, AW3D30, MERIT, TanDEM-X, SRTM, and NASADEM). *Remote Sens.* **2020**, *12*, 3482. [CrossRef]
62. Yan, Y.; Lidberg, W.; Tenenbaum, D.E.; Pilesjö, P. The Accuracy of Drainage Network Delineation as a Function of Environmental Factors: A Case Study in Central and Northern Sweden. *Hydrol. Process.* **2020**, *34*, 5489–5504. [CrossRef]
63. Wessel, B.; Huber, M.; Wohlfart, C.; Marschall, U.; Kosmann, D.; Roth, A. Accuracy Assessment of the Global TanDEM-X Digital Elevation Model with GPS Data. *ISPRS J. Photogramm. Remote Sens.* **2018**, *139*, 171–182. [CrossRef]
64. Souza, C.M., Jr.; Shimbo, J.Z.; Rosa, M.R.; Parente, L.L.; Alencar, A.A.; Rudorff, B.F.T.; Hasenack, H.; Matsumoto, M.; Ferreira, L.G.; Souza-Filho, P.W.M.; et al. Reconstructing Three Decades of Land Use and Land Cover Changes in Brazilian Biomes with Landsat Archive and Earth Engine. *Remote Sens.* **2020**, *12*, 2735. [CrossRef]
65. Speiser, J.L.; Miller, M.E.; Tooze, J.; Ip, E. A comparison of random forest variable selection methods for classification prediction modeling. *Expert Syst. Appl.* **2019**, *134*. [CrossRef]

**Disclaimer/Publisher’s Note:** The statements, opinions and data contained in all publications are solely those of the individual author(s) and contributor(s) and not of MDPI and/or the editor(s). MDPI and/or the editor(s) disclaim responsibility for any injury to people or property resulting from any ideas, methods, instructions or products referred to in the content.